Heliyon 9 (2023) e18486

Contents lists available at ScienceDirect

Heliyon

journal homepage: www.cell.com/heliyon

Comparative analysis of fracture characteristics between rock and rock-like materials

Xinnan Cui *, Jianming Wang, Bo Pan

Ansteel Beijing Research Institute, Beijing, 102211, China

A R T I C L E I N F O

Keywords:
Fracture toughness
Rock-like materials
Acoustic emission (AE)
Digital image correlation (DIC)
Semi-circular bending

A B S T R A C T

In order to investigate the characteristics of rock and rock-like materials during the fracture process, notched semi-circular bending (SCB) experiments of 3 rocks and 2 rock-like materials were conducted in this paper. The process of the crack mouth opening was measured with a clip gauge. Acoustic emission was used to analyze the damage and failure mode of the specimens. Meanwhile, the fracture process zone (FPZ) was analyzed with the digital image correlation (DIC). Finally, the differences in the fracture process between rocks and rock-like materials were observed with a polarized microscope, and the formation mechanism of FPZ was discussed. The results indicate that the sequence from brittleness to plasticity is gypsum, marble, granite, concrete and fine sandstone. The crack opening velocity of gypsum, marble, and granite reaches 0.02–0.025 mm/s, far exceeding that of sandstone and concrete at 0.003 mm/s and 0.005 mm/s. The stronger the brittleness of geomaterials, the less significant their acoustic emission effect. Only a few acoustic emissions occur during the fracture process of gypsum with 8 hits. Its fracture occurs instantaneously rather than through a process of damage to fracture and the failure mode is tensile failure. Sandstone has the strongest plasticity, with a large count of acoustic emissions before and after fracture, with a hit number of 5062, which is 630 times of pure gypsum. The fracture is a process of damage accumulation with 94% of sandstone, 89% of concrete, 80% of granite, and 60% of marble showing a tensile and shear failure mode except gypsum. In addition, the stronger the brittleness of geomaterials, the smaller their FPZ size. The FPZ of gypsum is only about 3 mm, which can be considered as lacking, while other materials are about 6–11 mm. The formation of FPZ depends on whether an interlocking structure can be formed inside the material, which is related to the base material and crystalline or aggregate particle size.

1. Introduction

Fracture mechanical properties including fracture toughness K_{IC}, fracture energy G_f, crack propagation process and fracture process zone are important contents of geotechnical materials [1]. As brittle materials, microcracks, joints and other defects are often contained in rocks, which leads to great differences in rock properties, especially in fracture mechanics [2].

Rock-like materials are usually composed of sand, stone, water, gypsum, resin, etc. with different proportions. The mechanical properties of these materials can be changed and controlled by adjusting the proportion, and the properties are relatively stable. Therefore, these synthetic materials such as concrete and gypsum are widely used as substitute materials of real rock in study of

* Corresponding author.
E-mail address: chester_tsui@sina.cn (X. Cui).

https://doi.org/10.1016/j.heliyon.2023.e18486
Received 26 April 2023; Received in revised form 20 June 2023; Accepted 19 July 2023
Available online 20 July 2023

fracture, damage, explosion, etc [3–5].

Concrete, widely used as a building material, its mechanical properties are similar to that of rocks, and it is often studied as rock substitute [6]. The mechanical properties as well as brittleness have been clearly discussed in literature [7–10]. It has been confirmed that DIC is an effective measurement method for crack propagation and fracture process zone analysis of concrete [11,12].

Concrete has high flexibility in model size, composition, internal structure. Therefore, it is widely used in the research of crack propagation, material fracture, throwing process, vibration in explosive engineering [13]. In liquid CO_2 blasting technology, the fracture process of concrete is often used to simulate that of rock, and the results are in good agreement with the results of on-site blasting [14].

In the uniaxial compression test of gypsum, the crack propagation process was also studied [15]. Two or more cracks are pre-arranged in the sample, and the propagation of multiple cracks was separated under uniaxial compression. The coalescence mechanism is connected, and the sample is finally damaged [16]. Similarly, the prismatic specimen made of gypsum mixture (cement and water) was also subjected to uniaxial compression test. The specimen was prefabricated with two non-parallel cracks, and the crack propagation sequence and mechanism were analyzed in detail [17,18]. Li et al. studied the fracture toughness of gypsum rock under real-time high-temperature conditions from 20 °C to 700 °C with semi-circular bending (SCB) experiment [19]. Fracture properties of gypsum interlayer in great depth in corrosive environments and a confining pressure were also studied [20,21]. Daniel et al. proposed several direct and indirect testing methods for gypsum fracture toughness [22]. The fracture behavior could be greatly altered by adding fibers, under three-point loading conditions, the reinforced gypsum shows a strong plasticity [23].

Other rock-like materials are mostly made of mixtures of several kinds of geotechnical materials, such as quartz sand, cement [24], diatomite, barite, resin [25]. The samples are made into cylinders and prisms with pre-designed cracks for uniaxial compression test.

As for real rocks, there are many kinds of research test methods. Commonly static methods such as uniaxial compression, triaxial compression, Brazilian splitting, three-point bending test [26], etc. The sample usually contains pre-processing cracks with diamond wire saw, ultra-thin saw blade, water jet, etc. Digital image correlation and acoustic emission are often used to observe fracture process zone [27] and failure process [28].

A variety of methods have been developed to measure the fracture mechanical properties of rocks with mode I cracks, including those based on short rod (SR) specimen, chevron bend (CB) specimen, notched Brazilian disk (NBD) specimen, cracked chevron-notched Brazilian disk (CCNBD) specimen, chevron-notched semi-circular bending (CNSCB) specimen and semi-circular bending (SCB) specimen. Research shows that the shape of the specimen, circular or semi-circular, the shape of the crack, chevron, straight edge will also affect the fracture toughness. Wei [29] compared the difference of mode I fracture toughness with different test methods.

The SCB specimen has been widely used for fracture toughness determination of geomaterials owing to inherent favorable properties such as its simplicity, minimal requirement of machining and the convenience of testing that can be accomplished by applying 3-point compressive loading using a common laboratory load frame [30]. Three-point impact of Brazilian disc with notch are usually preformed with SHPB equipment for dynamic fracture properties [31].

In previous researches, various loading methods have been used to study the mechanical properties of rocks or rock like materials. However, there is limited research on the comparison of fracture characteristics between natural rocks and rock like materials, the research on brittleness and plasticity of these geomaterials is also rare. Therefore, the SCB experiment recommended by ISRM has been conducted in this paper and the fracture characteristics of real rocks and rock like materials from multiple perspectives.

2. Experimental setup and data processing

2.1. Specimen preparation

All the specimens in this paper are SCB disks. The diameter of the specimen is 76 mm, the thickness is 30 mm. The notch is linear with a width of 1 mm, and depth of 15 mm, the ratio of notch length to radius a/R is 0.4, and the ratio of span to diameter $s/2R$ is 0.8, as

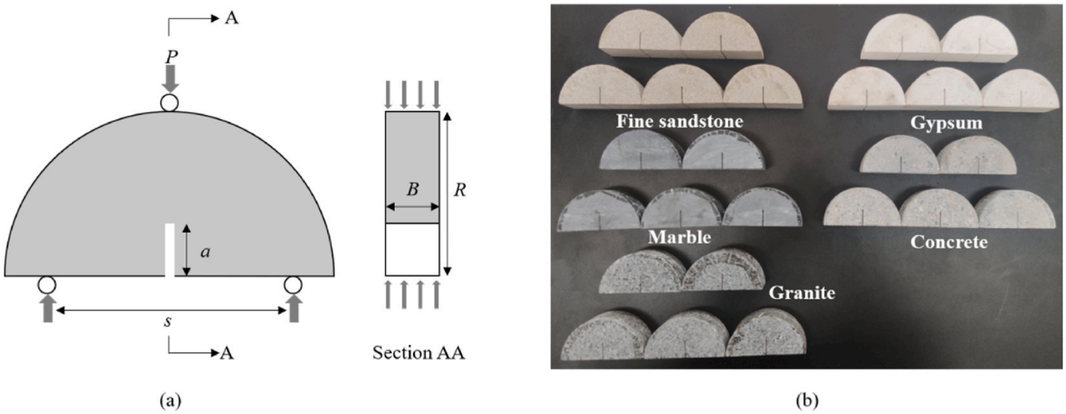

Fig. 1. The specimens. (a) Specimen structure. (b) Specimens of different types.

shown in Fig. 1 (a). The rock types are fine sandstone (from Zigong, Sichuan Province of China), marble (from Nanyang, Henan Province of China) and granite (from Rizhao, Shandong Province of China). The rock-like materials are gypsum and C30 concrete, as shown in Fig. 1 (b). The basic properties of the materials are shown in Table 1.

2.2. Experimental setup

The TAW-2000 rock mechanics testing machine was used in this experiment, as shown in Fig. 2. A load sensor with max range of 20 kN was equipped. The three-point bending loading method with a constant displacement rate of 0.1 mm/min was used to load all the SCB specimens. A clip gauge was attached to the bottom of the specimen to measure the crack mouth opening displacement. For each specimen type, 5 experiments were conducted at the same conditions. However, for each experiment, digital image correlation (DIC) method or acoustic emission (AE) method was applied for observation.

The experiment was conducted by the following steps:

(1) Place the specimen on the three-point bending fixture and adjust the position of the specimen to make the notch coincide with the centerline of the indenter;
(2) The specimen was symmetrically supported by two rollers with a span of 60 mm;
(3) Focus the lens and adjust the LEDs to make the image of the specimen clear if DIC method was used;
(4) Apply a preload of about 10 N to fix the specimen, and after that, the experiment could begin. The observation system (DIC or AE) should begin asynchronously with the testing machine and continue until the specimen fails.

2.2.1. DIC method

The DIC method is adopted to obtain the surface displacement and strain fields of the specimens. An open-source DIC algorithm *Ncorr* was used to calculate the displacement fields [32]. A Photron high-speed camera with a fixed focus lens was used for image acquisition at a frame rate of 60 fps. Specially, the frame rate for gypsum is 1000 fps due to the strong brittleness of gypsum. Two LED cold lights were equipped for the DIC system to maintain a constant lighting condition during the experiment as shown in Fig. 2. The resolution of the images is 1024 × 1024 pixels. The diameter of the specimen in the image is 415 pixels, that is, the resolution in image is 0.18 mm/pixel.

The speckles on the specimens were generated by the 'black and white painting' method with the following steps:

(1) Paint the surface of the specimen with a white paint as show in Fig. 3(a);
(2) Use a black paint to generate random ink dots and let them fall from 40 cm height as shown in Fig. 3(b). The average speckle size is 2–8 pixels.

The DIC system was calibrated with the Matlab Camera Calibrator Toolbox. A 12 × 9 checkboard pad with each was used and a total of 18 images were taken for system calibration as shown in Fig. 3(c). The overall mean error of the DIC system was 0.04 pixels by the calibration. That is, the displacement accuracy was 0.0072 mm.

2.2.2. AE method

Three nano-30 AE sensors were attached to the surface of the specimen as shown in Fig. 2. AE signals were amplified with 40 dB gain by preamplifier, and then recorded by AE measurement system (PCI-2, PAC). The AE waveform was recorded at 1 MHz sampling frequency. All the sensors were pasted with high vacuum grease.

3. Experimental results and analysis

3.1. Peak load

The load-displacement curves of all specimens are shown in Fig. 4. The result shows that concrete, gypsum, granite and marble show similar properties. Firstly, they show strong brittleness, and immediately fracture after the load reaches the peak. Secondly, the pre-peak stage can be divided into the compaction phase and elastic phase. In the compaction phase, the load curve presents a concave type, which shows that the microcracks in the specimens are closed. In the elastic phase, the load rises rapidly until the failure.

Table 1
Properties of specimen.

Specimen type	ρ (g·cm^{-3})	f_c (MPa)	f_t (MPa)	E (GPa)	V (m·s^{-1})
Fine sandstone	2.26	83.14	3.28	10.1	2531.65
Marble	2.62	141.32	6.85	72.91	5263.16
Granite	2.6	172.4	5.28	48.03	4081.63
Concrete	2.04	35.62	2.42	17.66	3773.58
Gypsum	1.12	15.95	1.28	3.85	2597.4

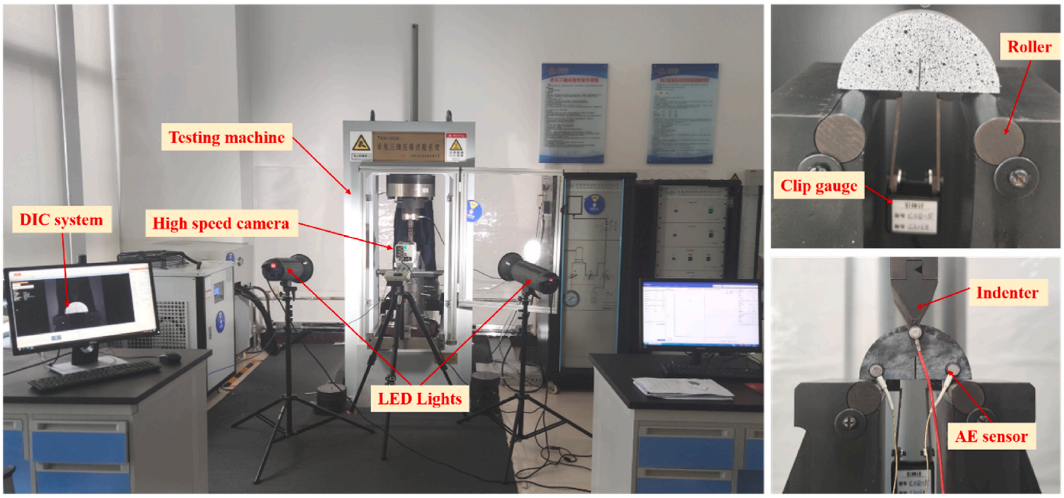

Fig. 2. The experimental setup and measuring methods.

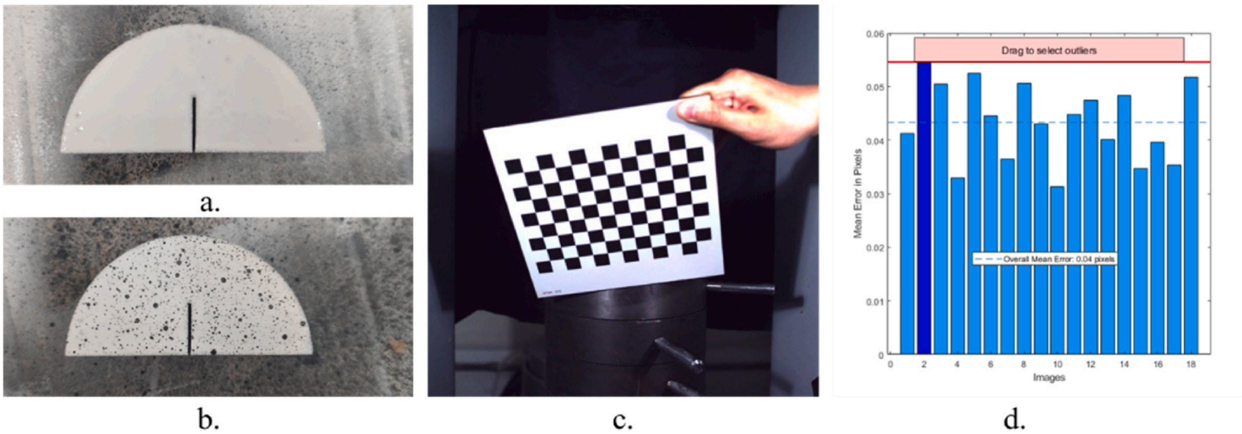

Fig. 3. The specimen preparation and system calibration: a. the specimen with white paint; b. the specimen with black speckles; c. the checkboard pad; d. the calibration result.

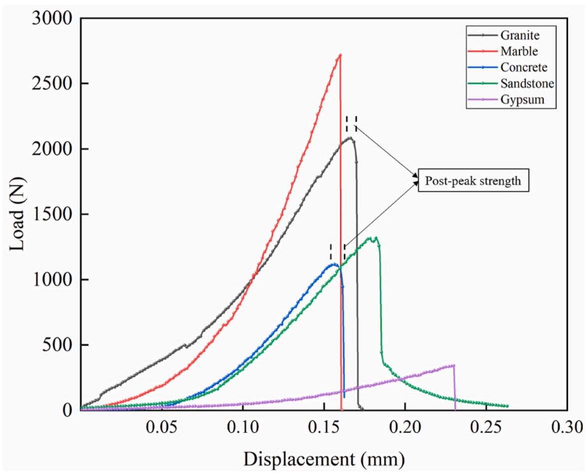

Fig. 4. The load-displacement curves of all specimens.

However, unlike marble and gypsum, concrete and granite have a certain post-peak strength.

The fine sandstone has a special property. The load falls rapidly after it reaches the peak, but the specimen still has a certain bearing capacity (maximum 440 N, 33.4% of the peak load), and a certain deformation capacity (0.08 mm, 30.4% of the total displacement). The pre-peak phase is similar to other materials.

3.2. Fracture toughness and energy

Model I fracture toughness K_{IC} of SCB specimen can be determined by the following formula [33]:

$$K_{IC} = Y\frac{P_{\max}\sqrt{\pi a}}{2RB} \tag{1}$$

$$Y = -1.297 + 9.516\frac{s}{2R} - \left(0.47 + 16.457\frac{s}{2R}\right)\frac{a}{R} + \left(1.071 + 34.401\frac{s}{2R}\right)\left(\frac{a}{R}\right)^2 \tag{2}$$

Where Y is the non-dimensional stress intensity factor (SIF) corresponding to the designed notch length a. In this experiment Y is 5.436.

The fracture energy G_f of SCB specimen can be obtained by the following formula [34]:

$$G_f = \frac{W_f}{A_{lig}} \tag{3}$$

Where $W_f = \int Pdu$ is the fracture work, P is the load and u is the displacement of load point. $A_{lig} = (R - a)\cdot B$ is the ligament.

The test results were shown in Table 2.

3.3. Crack opening process

The crack opening displacement in the test was measured with a clip gauge which was attached on the bottom of the specimen. The curves of crack opening displacement and load with time are shown in Fig. 5. The load curves have been discussed in Section 3.1.

Compared with the other four materials, fine sandstone has a longer elastic stage (from 19.5% pre-peak load, granite 30%, marble 28%, concrete 29.4%, gypsum 32.1%). For the crack opening process, fine sandstone is the most special. Its post-peak strength can last for a long time (46.5 s, 30% of the total time). The crack opening displacement (COD) at peak load is 0.071 mm, and the fracture COD reaches 0.43 mm, which is the largest. The fracture CODs of the other four samples are at the same level, granite 0.05 mm > concrete 0.03 mm > marble 0.02 mm = gypsum 0.02 mm. The fracture COD reflects the brittleness of the material. The smaller the COD is, the smaller plastic deformation and higher brittleness is.

The crack opening velocity (COV) is calculated according to COD. Except for fine sandstone, the crack propagates steadily at a velocity of 0.001 mm/s in the pre peak phase. When the load reaches the peak, the COV is the largest (marble 0.025 mm/s > gypsum 0.023 mm/s > granite 0.02 mm/s > concrete 0.005 mm/s).

Fine sandstone has strong plasticity comparatively. The COV before the peak load is 0.003 mm/s, the maximum COV reaches 0.102 mm/s at 43.8% post-peak, and then drop to 0.007 mm/s at 18.9% post-peak until completely fracture. The crack propagation process shows that gypsum, marble and granite show similar brittleness, and the COV before fracture is 0.02–0.025 mm/s. The COV concrete and sandstone is similar before the peak load, but sandstone has a post-peak strength.

3.4. Fracture process zone

To measure the length of FPZ, the position of FPZ tip must be defined. Two methods are commonly used for FPZ tip determination, the displacement method [27] and the strain method [35]. For geotechnical materials, the tensile strain bearing capacity could be defined as the maximum tensile strain in the crack opening direction before forming a crack. Therefore, when the strain around the crack tip reaches the tensile strain bearing capacity, this point is the FPZ tip. The tensile strain bearing capacity can be determined by the following formula:

$$\varepsilon_t = \frac{f_t}{E} \tag{4}$$

The displacement field and strain field corresponding to the peak load are obtained using the DIC method. The FPZ tips of the five

Table 2
Peak load and K_{IC} in SCB experiments.

Specimen type	Peak load (N)	K_{IC} (MPa·m$^{1/2}$)		G_f (J·m^{-2})	
Fs 1-5	1408.8, 1317.5, 1351.9, 1298.5, 1389.6	0.73, 0.68, 0.70, 0.67, 0.72	0.70	131.30, 123.48, 125.22, 122.03, 129.71	126.35
Ma 1-5	2757.3, 2718.4, 2714.7, 2770.1, 2702.3	1.43, 1.41, 1.40, 1.40, 1.43	1.41	191.88, 189.13, 187.83, 184.93, 190.58	188.87
Gr 1-5	2205.4, 2080.9, 2372.4, 2155.9, 2280.3	1.14, 1.08, 1.23, 1.12, 1.18	1.15	217.10, 211.88, 225.80, 214.78, 220.87	218.09
Co 1-5	1016.6, 1116.7, 1300.5, 1150.8, 1205.6	0.53, 0.58, 0.67, 0.60, 0.60	0.60	81.45, 88.12, 90.58, 83.77, 90.72	86.93
Gy 1-5	368.5, 309.3, 340.4, 333.5, 315.8	0.19, 0.16, 0.18, 0.17, 0.16	0.17	32.61, 34.49, 35.07, 32.90, 31.59	33.33

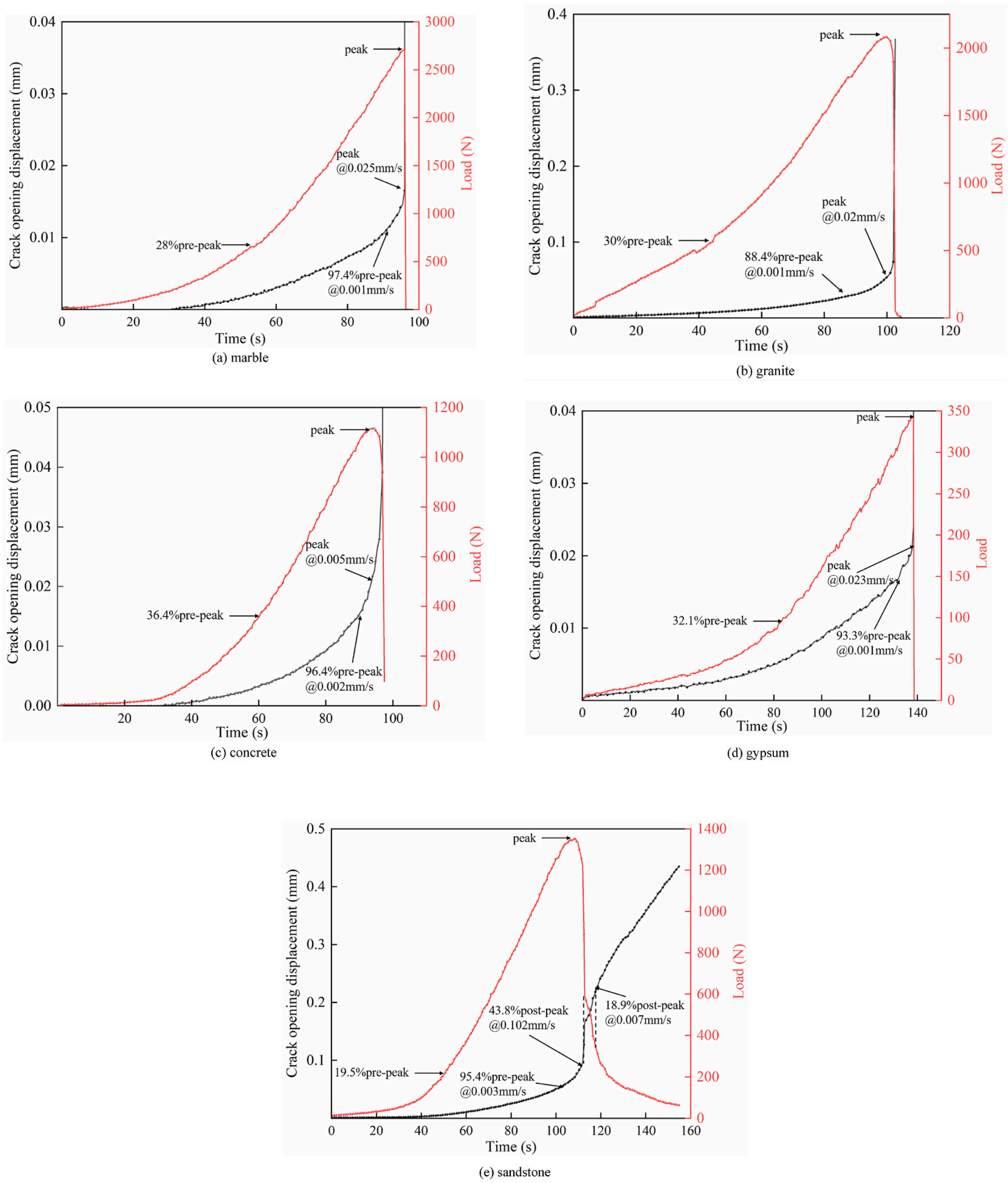

Fig. 5. The curves of crack opening displacement and load with time: a. marble; b. granite; c. concrete; d. gypsum; e. sandstone.

specimens were determined in the ε_{xx} fields, as shown in Fig. 6.

In addition, the critical FPZ length r_c could be estimated based on Schmidt's maximum principal stress model [36]:

$$r_c = \frac{1}{2\pi}\left(\frac{K_{IC}}{f_t}\right)^2 \tag{5}$$

Table 3 shows the FPZ length r determined with DIC strain method and theoretical length r_c with a relative error of 7.6%–16.6%. Compared to the DIC displacement method, the strain method for determining FPZ is simple and feasible with an acceptable accuracy.

As an inherent property of materials, the main factors affecting the size of FPZ are the particle size of the material and the size of the specimen. From this test, it can be seen that gypsum has the smallest FPZ size.

According to the previous analysis, gypsum has the strongest brittleness, and the fracture occurs almost instantaneously. The FPZ effect of gypsum is not obvious. The FPZs of the other four materials are similar. The result shows that FPZ has a certain correlation with the brittleness and plasticity of the materials. The stronger the brittleness, the less obvious the FPZ effect. On the contrary, the stronger the plasticity, the more obvious the FPZ effect.

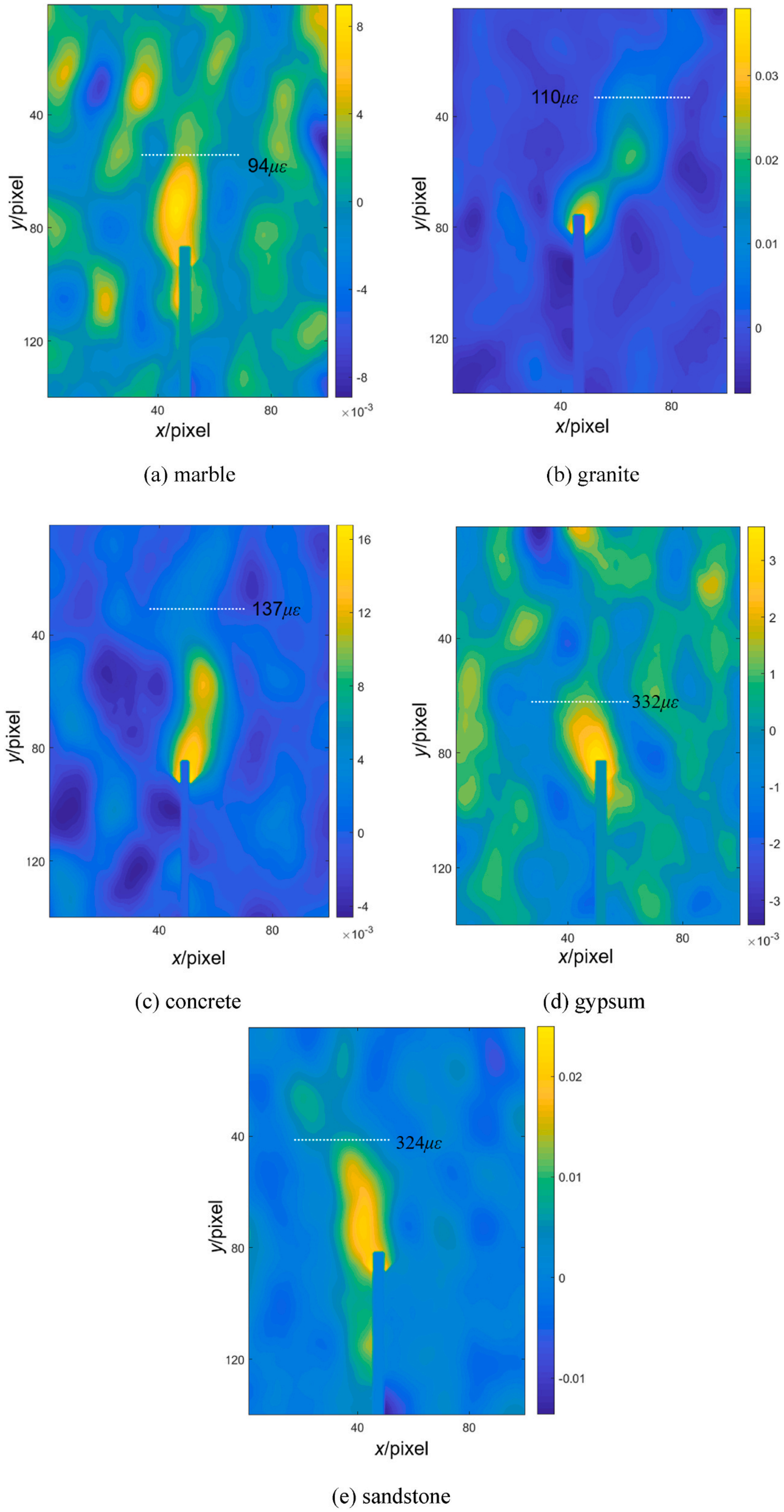

Fig. 6. The FPZ tips of all specimens in ε_{xx} field contour maps.

3.5. AE results

The failure process of the specimens was analyzed based on the acoustic emission parameter method. The cracks could be classified with RA and AF, which represents the specific value of rise time to amplitude and counts to duration respectively. High AF and low RA represent tensile cracks, and Low AF and high RA represent shear cracks [37]. Fig. 7 shows the RA-AF diagram of different materials. The data from the three acoustic emission sensors are basically the same. Therefore, the AE data of the middle sensor is taken for analysis, and the scattered point concentration area is enlarged. The hit counts during the destruction process are Sandstone 5062>Granite 2036>Concrete 765>Marble 355>Gypsum 8.

As an important precursor effect of material damage and failure, acoustic emission activity is closely related to the failure process. As shown in Fig. 7, the acoustic emission phenomenon of gypsum is not active during the test process, and there are only a few hits during the entire process, which is related to its strong brittleness. The failure mode of gypsum could be considered as pure tensile failure mode, while the rest of the materials are composite failure mode of tensile and shear. From the perspective of scattered point density, the tensile failure of marble and concrete is dominant, while the tensile and shear failure of sandstone and granite are equivalent. Based on the analysis of the crack propagation process, it can be concluded that the stronger the brittleness of the material, the less active the acoustic emission phenomenon, and the more likely the material is to undergo tensile failure mode. On the contrary, the stronger the plasticity of the material, the more active the acoustic emission phenomenon, and the failure mode tends to be a composite tensile and shear failure.

The damage D is defined based on the counts:

$$D = \frac{\sum_t C}{\sum C} \tag{6}$$

Where $\sum_t C$ is the accumulated counts at the current time, and $\sum C$ is accumulated counts at the failure time.

It could be inferred that the specific value of AF and RA, AR indicates the failure mode of the crack represented by the acoustic emission activity. A higher AR represents a tensile crack, while a lower AF represents a shear crack. The variation of AR and D over time of different materials is shown in Fig. 8.

As shown in Fig. 8, the acoustic emission activity of gypsum is concentrated at the failure moment, and there is no evidence of damage before failure. The maximum of AR value is 0.49 dB μs^{-2}. The AR values of the other materials are similar, ranging from 0–50 dB μs^{-2}. Except for gypsum, the failure of the sample is accumulation process of damage. The D value corresponding to the previous acoustic emission at the moment of peak load is sandstone 94%>concrete 89%>granite 80%>marble 60%. It can be inferred that the stronger the brittleness, the lower the damage before failure. In terms of time, sandstone has the strongest plasticity, and acoustic emissions are relatively more active throughout the test process, and there are still a large number of acoustic emission signals in the post-peak phase. The failure mode of the 4 materials is composite tensile and shear failure, however, in the failure phase, the scattered points with low AR are denser, indicating that the shear cracks are dominated in this phase.

4. Discussion on FPZ

Crack propagation in rock is characterized by the formation of microcracks around the crack tip, and interlocking in a portion of the crack where displacement have not reached a critical value. This zone of inelastic behavior is called the fracture process zone (FPZ), analogous to the plastic zone in metals. The FPZ was initially proposed in the study of granite fracture process [38].

Afterwards, FPZ was found in more rocks, and it was more evident in the fracture model of concrete. In the study of concrete fracture process, the size of FPZ in concrete is related to the maximum aggregate size [39]. It is generally accepted that the basic reason of FPZ in concrete is the interlocking structure of aggregates and the base at the crack front. In the FPZ, the strength was reduced. However, the tensile strain has not reached the critical value.

The Zeiss polarized light microscope was used to observe the interlocking structure during the crack propagation process which was widely present in natural rocks such as granite, sandstone and marble, mainly formed by the bonding between crystalline particles and the base, as shown in Fig. 9(a)~(c). In concrete, however, aggregates are added to form an artificial interlocking structure, which also endows the concrete with the characteristics of the fracture process zone in Fig. 9(d).

The prerequisite for the interlocking structure is the bonding between crystalline particles or aggregates and the base. Further observation shows that the larger the crystalline particles or aggregates, the greater the bonding force between them and the base, the greater the load-bearing capacity of the interlocking structure, and the larger the size of the fracture process zone.

Table 3
FPZ length r and r_c of specimens.

Specimen type	ε_t ($\mu\varepsilon$)	r(mm)	r_c(mm)	Relative error
Fine sandstone	324	8.46	7.26	16.6%
Marble	94	6.12	6.78	9.8%
Granite	110	8.12	7.53	7.6%
Concrete	137	11.16	9.76	14.3%
Gypsum	332	3.24	2.89	11.9%

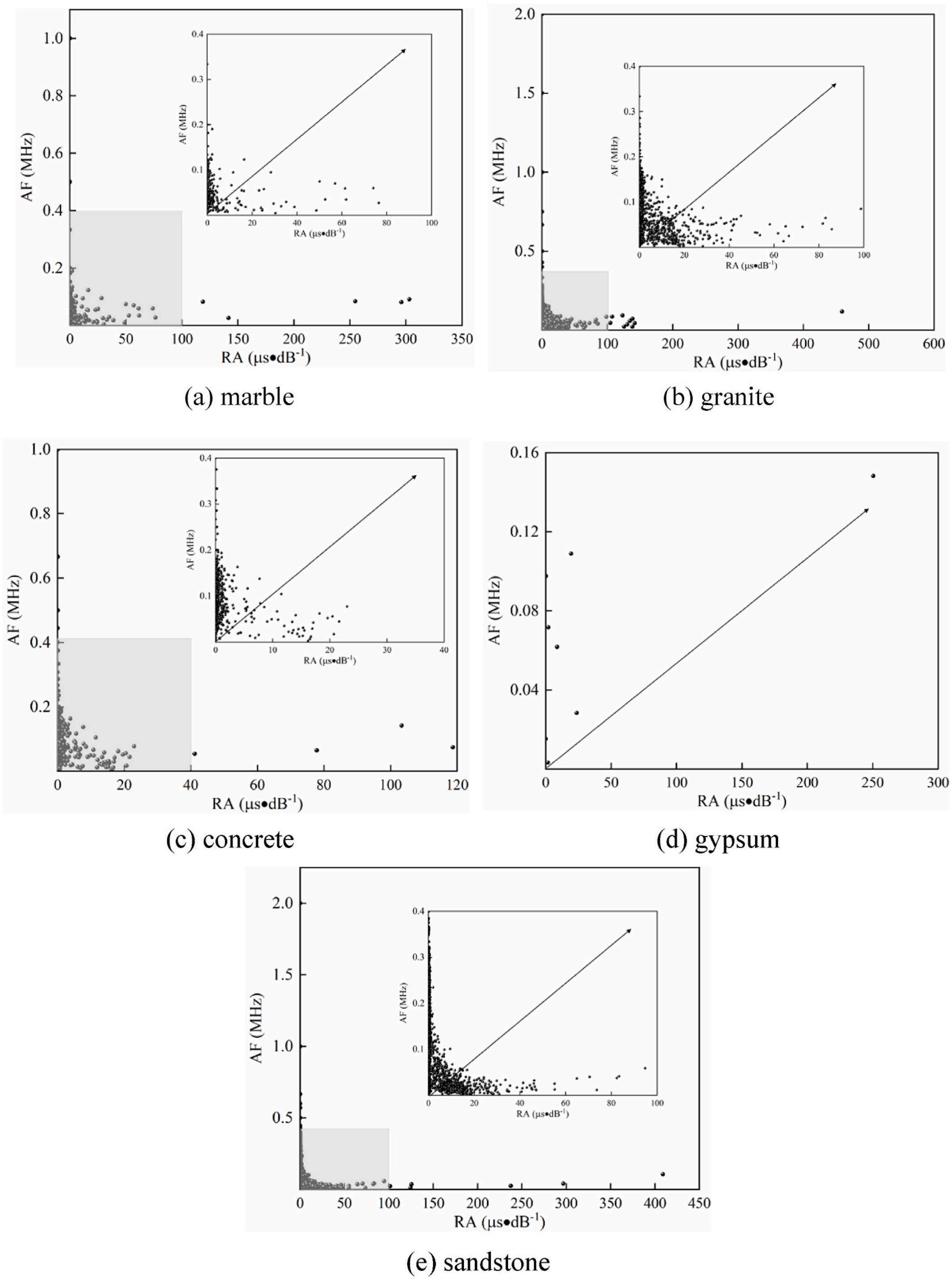

Fig. 7. Relationship of RA value and AF value of all materials.

However, without the addition of aggregates in gypsum, it is similar to a homogeneous material and interlocking structure cannot be observed. Therefore, it is reasonable to infer that there is no fracture process zone in gypsum.

Similarly, literature [40,41] observed a significant difference between pre-cracked marble and gypsum specimens under uniaxial loads. Before the development of observable cracks, macroscopic white patches were observed in marble, but not in gypsum with high-speed camera. Moreover, in microscopic scale observation with SEM and ESEM, the withe patch was associated to a micro-cracking zone around the crack path. The grain sizes of marble and gypsum were 50–250 μm and 5–20 μm respectively. In marble, the

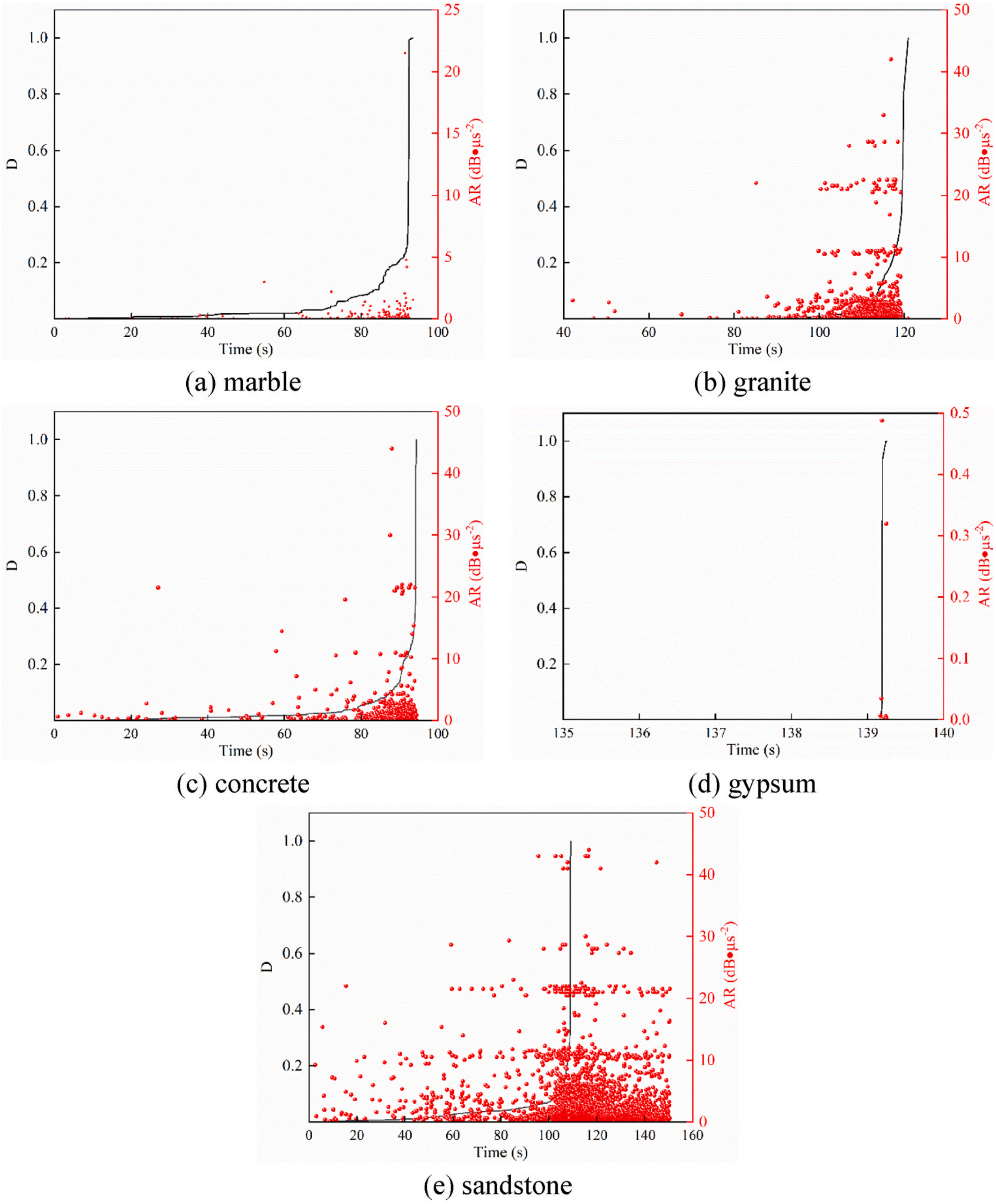

Fig. 8. Relationship of D value and AR value with time of all materials.

length of a microcrack was equal to or less than 1–2 grain sizes, making it easily to form high density microcracks (the which patch) on the flank of the central dominant microcrack. However, the microcracks in gypsum develop into a dominant microcrack at a length of 5–10 grain sizes rather than new microcracks in the vicinity. This difference leads to the different crack types. In marble, both inter-granular and intra-granular cracks are common. However, inter-granular cracks are common and it is difficult to determine the extent of intra-granular cracks development.

The results observed in the above literature are similar to those in this paper. It is reasonable to infer that the formation FPZ is related to the size of the microcracking zone which is associated to the grain size.

5. Conclusion

In the notched SCB experiments of five geotechnical materials, various properties of the failure process were analyzed with DIC and AE methods, respectively. The main conclusions are as follows:

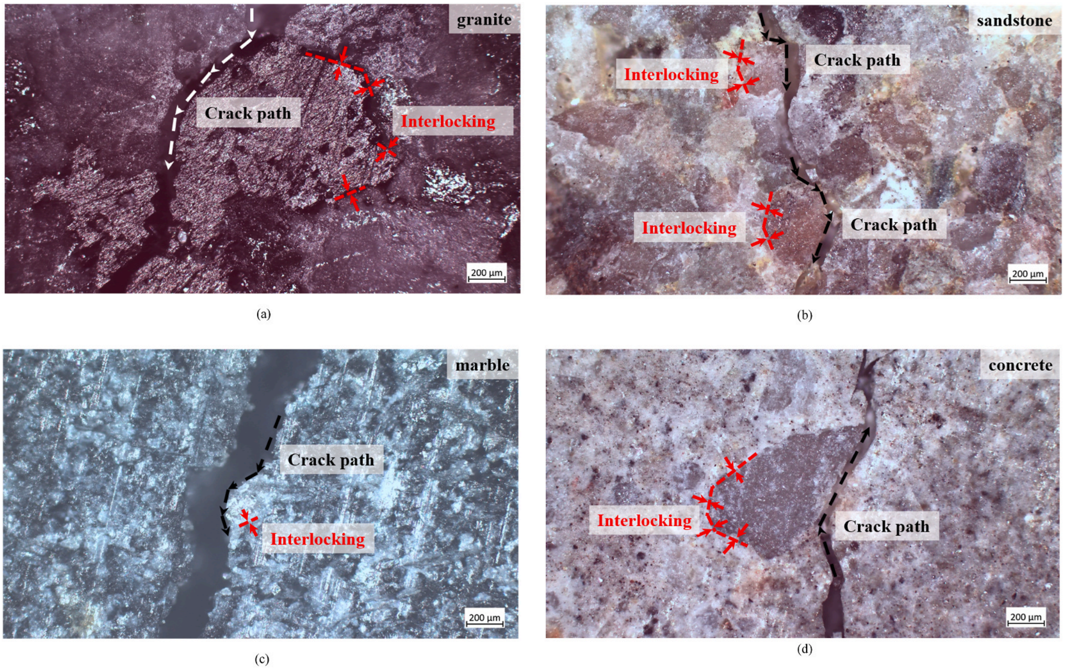

Fig. 9. The interlocking structure in natural rocks and concrete in microscopic images: a. granite; b. sandstone; c. marble; d. concrete.

(1) According to comprehensive analysis, the five geotechnical materials are gypsum, marble, granite, concrete, fine sandstone from brittleness to plasticity. The fracture process, especially the crack propagation process, varies greatly among different materials. The stronger the brittleness of a material, the more sudden its failure is, and the fewer the omens of failure. In AE test, the strong brittleness of gypsum makes its failure occur instantaneously, the hit is 1/44 of marble, which with similar brittleness, and only 1/630 of sandstone. There is no damage before failure in gypsum.
(2) The stronger the brittleness of the material, the faster the crack opening velocity during its failure. The crack opening velocity of gypsum, marble and granite reaches 0.02–0.025 mm/s, which is much higher than 0.003 mm/s and 0.005 mm/s of sandstone and concrete.
(3) The formation of FPZ was discussed in this paper. The interlocking structure formed by the bonding between crystalline particles or aggregates and the base, which hinders the macro crack propagation, is the mainly formation of FPZ. There is no fracture process zone in homogeneous materials such as gypsum.
(4) Appropriate materials should be selected based on the properties of natural rocks in analogical simulating tests. Concrete is suitable for replacing most rocks. Moreover, the characteristics of gypsum could be changed by adding mineral particles, making it suitable as a substitute for rocks with strong brittleness and other properties such as FPZ effect.

Author contribution statement

Xinnan Cui: Conceived and designed the experiments; Performed the experiments; Analyzed and interpreted the data; Contributed reagents, materials, analysis tools or data; Wrote the paper.

Jianming Wang: Performed the experiments; Analyzed and interpreted the data.

Bo Pan: Performed the experiments.

Declaration of competing interest

The authors declare that they have no known competing financial interests or personal relationships that could have appeared to influence the work reported in this paper.

Acknowledgements

The authors would like to thank Ansteel Group for the scientific research supports.

References

[1] S. Miao, P.Z. Pan, P. Yu, et al., Fracture analysis of Beishan granite after high-temperature treatment using digital image correlation, Eng. Fract. Mech. 225 (1–2) (2019), 106847, https://doi.org/10.1016/j.engfracmech.2019.106847.

[2] J.Z. Zhang, X.P. Zhou, J.Y. Zhu, et al., Quasi-static fracturing in double-flawed specimens under uniaxial loading: the role of strain rate, Int. J. Fract. 211 (2018) 75–102, https://doi.org/10.1007/s10704-018-0277-8.

[3] S. Mansour, L.M. Shen, Q.F. Xu, Characterisation of mechanical behaviour of 3D printed rock-like material with digital image correlation - ScienceDirect, Int. J. Rock Mech. Min. Sci. 112 (2018) 122–138, https://doi.org/10.1016/j.ijrmms.2018.10.012.

[4] S. Huang, Y. Liu, Y. Guo, et al., Strength and failure characteristics of rock-like material containing single crack under freeze-thaw and uniaxial compression, Cold Reg. Sci. Technol. 162 (2019) 1–10.

[5] X.N. Cui, X.G. Wang, Y.J. Wang, et al., External crack propagation of concrete surface under explosive loading, Explos. Shock Waves 40 (5) (2020), 25-3 (in Chinese) Doi: 10.11883/bzycj-2019-0364.

[6] L.Y. Yang, H.Z. Xie, S.Z. Fang, et al., Experimental study on mechanical properties and damage mechanism of basalt fiber reinforced concrete under uniaxial compression, Structures (31) (2021) 330–340, https://doi.org/10.1016/j.istruc.2021.01.071.

[7] G.L. Golewski, Mechanical properties and brittleness of concrete made by combined fly ash, silica fume and nanosilica with ordinary Portland cement[J], AIMS Mater. Sci 10 (3) (2023) 390–404, https://doi.org/10.3934/matersci.2023021.

[8] G.L. Golewski, Fracture performance of cementitious composites based on quaternary blended cements, Materials 15 (2022) 6023, https://doi.org/10.3390/ma15176023.

[9] G.L. Golewski, The phenomenon of cracking in cement concretes and reinforced concrete structures: the mechanism of cracks formation, causes of their initiation, types and places of occurrence, and methods of detection—a review, Buildings 13 (2023) 765, https://doi.org/10.3390/buildings13030765.

[10] G.L. Golewski, B. Szostak, Strength and microstructure of composites with cement matrixes modified by fly ash and active seeds of C-S-H phase, Struct. Eng. Mech. 82 (4) (2022) 543–556, https://doi.org/10.12989/sem.2022.82.4.543.

[11] G.L. Golewski, An extensive investigations on fracture parameters of concretes based on quaternary binders (QBC) by means of the DIC technique, Construct. Build. Mater. 351 (2022), 128823, https://doi.org/10.1016/j.conbuildmat.2022.128823.

[12] G.L. Golewski, Comparative measurements of fracture toughgness combined with visual analysis of cracks propagation using the DIC technique of concretes based on cement matrix with a highly diversified composition, Theor. Appl. Fract. Mech. 121 (2022), 103553, https://doi.org/10.1016/j.tafmec.2022.103553.

[13] W.C. Zhu, D. Gai, C.H. Wei, et al., High-pressure air blasting experiments on concrete and implications for enhanced coal gas drainage, J. Nat. Gas Sci. Eng. 36 (2016) 1253–1263, https://doi.org/10.1016/j.jngse.2016.03.047.

[14] Y.N. Zhang, J.R. Deng, H.W. Deng, et al., Peridynamics simulation of rock fracturing under liquid carbon dioxide blasting, Int. J. Damage Mech. 28 (2018) 1038–1052, https://doi.org/10.1177/1056789518807532.

[15] C.H. Park, A. Bobet, Crack initiation, propagation and coalescence from frictional flaws in uniaxial compression, Eng. Fract. Mech. 77 (14) (2010) 2727–2748, https://doi.org/10.1016/j.engfracmech.2010.06.027.

[16] Y.H. Huang, S.Q. Yang, W.L. Tian, et al., An experimental study on fracture mechanical behavior of rock-like materials containing two unparallel fissures under uniaxial compression, Acta Mech. 32 (2016) 442–445, https://doi.org/10.1007/s10409-015-0489-3.

[17] L.O. Afolagboye, J. He, S. Wang, Experimental study on cracking behaviour of moulded gypsum containing two non-parallel overlapping flaws under uniaxial compression, Acta Mech. 33 (2017) 394–405, https://doi.org/10.1007/s10409-016-0624-9.

[18] C. Zhao, Y.M. Zhou, Cf Zhao, et al., Cracking processes and coalescence modes in rock-like specimens with two parallel pre-existing cracks, Rock Mech. Rock Eng. 51 (2018) 3377–3393, https://doi.org/10.1007/s00603-018-1525-y.

[19] C. Li, Y. Hu, T. Meng, et al., Mode-I fracture toughness and mechanisms of Salt-Rock gypsum interlayers under real-time high-temperature conditions, Eng. Fract. Mech. 240 (11) (2020), 107357, https://doi.org/10.1016/j.engfracmech.2020.107357.

[20] T. Meng, Y. Hu, R. Fang, et al., Study of fracture toughness and weakening mechanisms in gypsum interlayers in corrosive environments, J. Nat. Gas Sci. Eng. 26 (2015) 356–366, https://doi.org/10.1016/j.jngse.2015.06.027.

[21] T. Meng, D. Hua, Y.Q. Zhang, et al., Study of the deformation characteristics and fracture criterion of the mixed mode fracture toughness of gypsum interlayers from Yunying salt cavern under a confining pressure, J. Nat. Gas Sci. Eng. 58 (2018), https://doi.org/10.1016/j.jngse.2018.07.020.

[22] P. Daniel, M.R.M. Aliha, H.G. Kucheki, et al., Tensile and tear-type fracture toughness of gypsum material: direct and indirect testing methods, J. Rock Mech. Geotech. (2023), https://doi.org/10.1016/j.jrmge.2022.11.016.

[23] F. Suárez a, L. Felipe-Sesé a, F.A. Díaz b, et al., On the fracture behaviour of fibre-reinforced gypsum using micro and macro polymer fibres, Construct. Build. Mater. 244 (2020), https://doi.org/10.1016/j.conbuildmat.2020.118347.

[24] Y.H. Huang, S.Q. Yang, W. Zeng, Experimental and numerical study on loading rate effects of rock-like material specimens containing two unparallel fissures, J. Cent. South Univ. 23 (2016) 1474–1485, https://doi.org/10.1007/s11771-016-3200-3.

[25] X.P. Zhou, Y.T. Wang, J.Z. Zhang, et al., Fracturing behavior study of three-flawed specimens by uniaxial compression and 3D digital image correlation: sensitivity to brittleness, Rock Mech. Rock Eng. 52 (2019) 691–718, https://doi.org/10.1007/s00603-018-1600-4.

[26] T.Y. Guo, L.N. Wong, Z.J. Wu, Microcracking behavior transition in thermally treated granite under mode I loading, Eng. Geol. 282 (2021), 105992, https://doi.org/10.1016/j.enggeo.2021.105992.

[27] S. Zhang, H.Y. Wang, X.J. Li, et al., Experimental study on development characteristics and size effect of rock fracture process zone, Eng. Fract. Mech. 241 (2021), 107377, https://doi.org/10.1016/j.engfracmech.2020.107377.

[28] X.P. Zhou, J.Z. Zhang, F. Berto, Fracture analysis in brittle sandstone by digital imaging and AE techniques: role of flaw length ratio, J. Mater. Civ. Eng. 32 (5) (2020), 04020085, https://doi.org/10.1061/(ASCE)MT.1943-5533.0003151.

[29] M.D. Wei, F. Dai, Y. Liu, et al., Influences of loading method and notch type on rock fracture toughness measurements: from the perspectives of T-stress and fracture process zone, Rock Mech. Rock Eng. 54 (2021) 4965–4986, https://doi.org/10.1007/s00603-021-02541-9.

[30] Y.X. Zhou, K. Xia, X.B. Li, et al., Suggested methods for determining the dynamic strength parameters and mode-I fracture toughness of rock materials, Int. J. Rock Mech. Min. 49 (2012) 105–112, https://doi.org/10.1016/j.ijrmms.2011.10.004.

[31] Q.B. Zhang, J. Zhao, Quasi-static and dynamic fracture behaviour of rock materials: phenomena and mechanisms, Int. J. Fract. 189 (1) (2014) 1–32, https://doi.org/10.1007/s10704-014-9959-z.

[32] J. Blaber, B. Adair, A. Antoniou, Ncorr: open-source 2D digital image correlation Matlab software, Exp. Mech. 55 (2015) 1105–1122, https://doi.org/10.1007/s11340-015-0009-1.

[33] M.D. Kuruppu, Y. Obara, M.R. Ayatollahi, et al., ISRM-suggested method for determining the mode I static fracture toughness using semi-circular bend specimen, Rock Mech. Rock Eng. 47 (2014) 267–274, https://doi.org/10.1007/s00603-013-0422-7.

[34] D.C. Feng, S.T. Cui, J.Y. Yi, et al., Evaluation index of low-temperature asphalt mixture performance based on semi-circular bending test, China J. Highw. Transp. 33 (7) (2020) 50–57, https://doi.org/10.19721/j.cnki.1001-7372.2020.07.005 (In Chinese).

[35] S.Y. Alam, J. Saliba, A. Loukili, Fracture examination in concrete through combined digital image correlation and acoustic emission techniques, Construct. Build. Mater. 69 (2014) 232–242, https://doi.org/10.1016/j.conbuildmat.2014.07.044.

[36] E.Q. Li, J.L. Feng, T.Y. Zhu, et al., Examining type I fracture characteristics in layered slates with digital image correlation, J. Mining Safety Eng. 38 (5) (2021) 979–987, https://doi.org/10.13545/j.cnki.jmse.2020.0375 (In Chinese).

[37] Y.X. Zhao, Z. Sun, B. Liu, Comparative study of semi-circular bending tests for modes I and II fracture characteristics of Xinzhouyao bituminous coal, Chin. J. Rock Mech. Eng. 38 (8) (2019) 1593–1604, https://doi.org/10.13722/j.cnki.jrme.2019.0306 (In Chinese).

[38] J.F. Labuz, S.P. Shah, C.H. Dowding, Experimental analysis of crack propagation in granite, Int. J. Rock Mech. Min. Sci. Geomech. Abstracts 22 (2) (1985) 85–98, https://doi.org/10.1016/0148-9062(85)92330-7.

[39] Y.H. Zhao, The Analytical Study on the Energy in the Fracture Process of Concrete, 2002. Dalian University of Technology.
[40] L.N.Y. Wong, H.H. Einstein, Crack coalescence in molded gypsum and carrara marble: Part 1—macroscopic observations and interpretation, Rock Mech. Rock Eng. 42 (2009) 475–511, https://doi.org/10.1007/s00603-008-0002-4.
[41] L.N.Y. Wong, H.H. Einstein, Crack coalescence in molded gypsum and carrara marble: Part 2—microscopic observations and interpretation, Rock Mech. Rock Eng. 42 (2009) 513–545, https://doi.org/10.1007/s00603-008-0003-3.